

Surface state charge dynamics of a high-mobility three dimensional topological insulator

Jason N. Hancock¹, J. L. M. van Mechelen¹, Alexey B. Kuzmenko¹, Dirk van der Marel¹, C. Brüne², E. G. Novik², G. V. Astakhov², H. Buhmann², Laurens Molenkamp²

¹ *Département de Physique de la Matière Condensée, Université de Genève, quai Ernest-Ansermet 24, CH 1211 Genève 4, Switzerland and*

² *Physikalisches Institut der Universität Würzburg - 97074 Würzburg, Germany*

(Dated: June 4, 2022)

Spin 1/2 particles exhibit a counterintuitive property that their wavefunction acquires a π phase upon 360° rotation. If spin and orbital degrees of freedom are mixed in a particular way, the momenta of electrons in a crystalline lattice feel important effects of this π ‘Berry’s phase’, which can lead to a new phase of matter whose description requires a fundamental redress of the theory of semiconductors [1–3], and probably many other materials classes [4–6]. These topological insulators exhibit an odd number of metallic surface bands with helical spin texture [7–9] surrounding the nominally insulating bulk and display characteristic suppression of backscattering from step edges and nonmagnetic impurities [10, 11]. We present magneto-optical measurements deep in the terahertz frequency regime exploring the charge dynamics of surface states in high-mobility strained films of HgTe [12–15]. Using a time-domain technique, we detect a strong magneto-optical signal which is dominated by surface bands. This information reveals precise details of the low-energy excitations and momentum-energy dispersion of the helical metallic surface state.

The observation of the quantum spin Hall effect (QSHE) in CdTe-HgTe-CdTe quantum wells [16, 17] represents a significant advance in the ability to robustly segregate electronic currents of opposite spin, an effect which paves the way to new applications for spintronics and fault-tolerant quantum computation. In bulk, HgTe possesses the band inversion property due to spin-orbit interaction, a prerequisite condition for the QSHE, but also needed to realize a three dimensional topological insulator phase. Unfortunately, the Fermi level appears directly at the intersection of two bands, rendering the bulk semimetallic and leaving the surface states and the expected topological aspects of this material obscured by the low-energy bulk excitations. However, when HgTe is compressively strained against a CdTe substrate, the bulk band intersection becomes fully gapped in response to the lowered symmetry, permitting isolated access to helical surface bands [12–15]. Recently, strong evidence for the existence of the π Berry’s phase, surface bands, and associated zero Landau level were observed as a

quantum Hall effect of surface states, whose existence were subsequently verified using angle-resolved photoemission [15].

In order to probe directly the surface states of strained HgTe, we have developed a method of acquiring time-domain terahertz magneto-optical data using a home-built superconducting magnet in a flow cryostat, illustrated in Figure 1a. At 4.35 K, the magnetic field and incident polarizer angle θ_P were set, and one direct pulse plus one echo, due to internal reflection inside the substrate, were collected for analyzer angles θ_A subtending 400° in 10° steps. The pulse and echo were then partitioned into $E_1(t, \theta_A, B)$ and $E_2(t, \theta_A, B)$ as shown in Figure 1b, and separately Fourier transformed to obtain the electric field amplitudes $E_1(\omega, \theta_A, B)$ and $E_2(\omega, \theta_A, B)$.

When the pulse passes through or reflects from the film, the electric field direction can rotate due to off-diagonal elements of the dielectric tensor or possibly the predicted topological magneto-electric effect [18]. Accounting for the horizontally-polarizing detector and emitter antenna of the spectrometer, the electric field amplitude in pulse i at the detector is

$$E_i = E_s \cos \theta_P \cos \theta_A \cos(\theta_A - \theta_P + \theta_{F,i}) \quad (1)$$

where E_s is the electric field generated by the source and $\theta_{F,i}$ is the complex, sample-induced Faraday rotation of the i th pulse. Figure 1d,e shows an example fit of the intensity to the second pulse for fields of ± 1.4 T. The change in shape of the intensity distribution around 35 cm^{-1} is caused by a change in the complex Faraday angle at this frequency, which we attribute to an absorptive transition among surface state Landau levels.

The simultaneous acquisition of multiple pulses with separate histories of contact with the film provides an advantage in accurately determining the polarization rotation. Any polarizing effects of the polyethylene cryostat windows, as well as inaccuracy in repositioning the polarizer following an angle sweep is exactly the same for the two pulses, so taking the difference in the two Faraday angles $\theta_K = \theta_{F,2} - \theta_{F,1}$ cancels these extraneous effects. The normal-incidence Kerr angle θ_K , shown in Figure 1e and 2a-b is precisely the rotation of polarization induced when the pulse reflects at normal incidence from the substrate side of the film (Fig. 1d), and the accuracy to which it can be determined is greater than

for the Faraday angles separately.

The field-induced changes in θ_K are typical of cyclotron resonance (CR) behavior, for which the dynamical conductivity appropriate for photon angular momentum either parallel (+) or antiparallel (-) the momentum of the incident photon is:

$$\sigma_{\pm}(\omega) = i \frac{e^2}{h} \sum_j \frac{\omega_f^j}{\omega \pm \omega_c^j + i\gamma} \quad (2)$$

where ω_c^j is the cyclotron frequency, ω_f^j the Drude weight, and γ^j is the inverse lifetime of the j th band. While we explore the possibility of a multi-component CR below, the resonance is fit and satisfactorily described by a single effective ω_c , γ , and ω_f . The elementary response functions in Equation (2) are then used in concert with the transfer-matrix method for the substrate+film system (see Supplemental Materials). The Faraday angles are then obtained via Eqn. (1) and θ_K calculated and fit with the adjustable parameters summarized in Figures 2c-e. The sign of the rotation indicates that the carriers involved in the CR are electron-like, and fits to the field dependence give $\hbar\gamma = 0.9$ meV, a field-linear cyclotron frequency with $\hbar\omega_c/B = 2.92 \pm 0.02$ meV/T, and total Drude weight $\hbar\omega_f = 79.0 \pm 1.7$ meV. Using the relation $\mu B = \omega_c/\gamma$, and the nearly field-independent γ (Figure 2d), these fits imply a very high carrier mobility $\mu = 34,220$ cm²/V·s, consistent with previous transport [15] and optical [19] measurements.

In the limit of small carrier concentration, which as we will see below is the relevant limit in the context of this discussion, the 2D Fermi-surfaces are isotropic, and ω_f^j and ω_c^j at low fields are uniquely determined by the Fermi momentum, k_F^j , and the group velocity at the Fermi energy, v_F^j (see Supplemental Information)

$$\begin{aligned} \omega_f^j &= \frac{1}{2} v_F^j k_F^j \\ \omega_c^j &= \frac{eB}{\hbar} \frac{v_F^j}{k_F^j} \end{aligned}$$

Knowledge of ω_f^j and ω_c^j therefore permits determination of the parameters v_F^j and k_F^j , which in turn provides valuable and precise information on the band structure at and around the Fermi energy.

In our 70 nm films, the conduction band is quantized and well-separated in energy due to confinement in the z direction, and any possible bulk contributions come from a small number of two-dimensional electron pockets. Unlike bulk, the surface contributions to the Drude weight are present for all values of the chemical potential, due to their gapless nature. Because the surface bands are at higher filling ($k_F^s > k_F^b$) and are more steeply dispersing ($v_F^s > v_F^b$) than the conduction bands, these states not only always contribute to the CR, but also always con-

tribute more strongly to the magneto-optical signal than a set of bulk states with the same Fermi surface area.

Before we address the implications of possible contributions from the bulk, we start with the simplest assumption, namely that the only contributions to the observed Kerr rotation originate from the two surfaces of the film with approximately the same charge carrier concentration. This is motivated by the magneto-transport showing a quantized Hall effect that results from the 2D Dirac-like topological surface states with densities 4.8×10^{11} cm⁻² and 3.7×10^{11} cm⁻² for the CdTe and vacuum interfaces (respectively) and negligible contribution from the bulk [15]. Since with this assumption $\hbar\omega_f^j = 38.5 \pm 0.9$ meV for the two surfaces, combination with ω_c/B gives $v_F^s = 5.88 \times 10^5$ m/s and $k_F^s = 0.201$ nm⁻¹ (see Fig 3a). The corresponding carrier concentration per surface is $n_{2D} = k_F^2/(4\pi) = 3.2 \times 10^{11}$ cm⁻² in good agreement with the high field transport data. The remaining difference is within the observed variations from one cool-down to another of the same sample, which we attribute to molecular adsorption at the surface of the film at cryogenic temperatures. Comparing these k_F values with the quantum well bandstructure in [15], the level of the chemical potential should be positioned above the conduction band bottom with 25% of the Drude weight arising from the bulk states of the film, with the remainder due to the surface bands. Attributing only 75% of the observed Drude weight to the surface states would result in: $v_F^s = 5.09 \times 10^5$ m/s and $k_F^s = 0.174$ nm⁻¹. These values are indicated as the dotted lines in Fig. 3a. Angle-resolved photoelectron spectroscopy shows a linear dispersion down to 1 eV below the Fermi energy with a velocity 4.3×10^5 m/s [15]. The somewhat higher value obtained from the optical data is expected, since this probes the velocity at the Fermi energy which is closer to the light conduction bands hybridizing with the 2D surface states.

More detailed knowledge of our surface-dominated cyclotron resonance can be gained from use of a surface state model dispersion relation $\epsilon_k = E_{DP} + Ak + C_2k^2$ [20]. This form accommodates the topologically protected Dirac point (DP) through the A term, but allows for significant deviations from the ideal conical dispersion through the C_2 term. By varying these parameters, one can interpolate continuously between a pure Dirac cone ($C_2 \rightarrow 0$) and a parabola ($A \rightarrow 0$) emanating from the Dirac point at zone center and energy E_{DP} lying inside the bulk gap. All of the curves of this type with the same values of k_F and v_F fit equally well to our data, as shown in Figure 3b. However, in order to place the DP inside the bulk gap, estimated to be ~ 26 meV at zone center, the A parameter must be very small, $A < 50$ meV·nm, in order to be consistent with our data. The resultant parameter C_2 is therefore quite large in comparison to other topological materials [7–9, 20], indicating a relatively rapid departure from the ideal conical dispersion near the DP

in strained HgTe. The large second-order term leads one to suspect that higher order isotropic terms (k^3 , k^4 , ...) may be necessary for detailed analysis of certain experiments.

While we do not measure the Fermi energy directly, the simplified dispersion analysis above puts the chemical potential within 40 meV of the Dirac point. This difference can be overcome through gating in an appropriate experimental design, and the chemical potential can be tuned near the Zeeman split zero Landau level. This would fulfill the conditions required to observe the predicted topological magnetoelectric coupling effect [18] as a quantized Kerr rotation. This long-sought effect bears close mathematical analogy to high-energy particle theory, permitting one to use terahertz spectroscopy to study the properties of an ‘axion’ domain wall [21], and the methods developed here are highly suited for this pursuit.

We have studied the low energy electrodynamics of topological surface states of strained HgTe using a novel time-domain magneto-optical spectroscopic technique providing Kerr angle spectra to very low energies (<1 meV). The method allowed us to obtain the parameters describing the topological surface states near the Fermi energy, until now not resolved by other experimental techniques, namely free carrier spectral weight, quasi-particle scattering rate, cyclotron frequency, Fermi-velocity and Fermi-momentum. Taken together with the requirement that the Dirac point must lie inside the bulk gap, our results imply that the surface bands of strained HgTe are markedly nonconical.

METHODS

High mobility, 70 nm HgTe film sample was grown on a thick CdTe substrate using molecular beam epitaxy, and characterized by X-ray, ARPES, and d. c. transport measurements. The finite area of the film, 4×5 mm, limits the lowest measurable frequency in our measurements. Time-domain terahertz traces were collected with a commercial system employing a mode-locked laser and photoconducting antennae.

ACKNOWLEDGEMENTS

We acknowledge valuable discussions with Shoucheng Zhang and Alberto Morpurgo. This work is supported by the SNSF through Grant No. 200020-130052 and the National Center of Competence in Research (NCCR) MaNEP.

-
- [1] C. L. Kane and E. J. Mele, Phys. Rev. Lett. **95**, 226801 (2005).
 - [2] H. Zhang, C.-X. Liu, X.-L. Qi, X. Dai, Z. Fang, and S.-C. Zhang, Nat Phys **5**, 438 (2009), URL <http://dx.doi.org/10.1038/nphys1270>.
 - [3] M. Z. Hasan and C. L. Kane, Rev. Mod. Phys. **82**, 3045 (2010).
 - [4] S. Raghu, X.-L. Qi, C. Honerkamp, and S.-C. Zhang, Phys. Rev. Lett. **100**, 156401 (2008).
 - [5] C. W. Groth, M. Wimmer, A. R. Akhmerov, J. Tworzycylo, and C. W. J. Beenakker, Phys. Rev. Lett. **103**, 196805 (2009).
 - [6] M. Dzero, K. Sun, V. Galitski, and P. Coleman, Phys. Rev. Lett. **104**, 106408 (2010).
 - [7] D. Hsieh, D. Qian, L. Wray, Y. Xia, Y. S. Hor, R. J. Cava, and M. Z. Hasan, Nature **452**, 970 (2008), URL <http://dx.doi.org/10.1038/nature06843>.
 - [8] D. Hsieh, Y. Xia, D. Qian, L. Wray, J. H. Dil, F. Meier, J. Osterwalder, L. Patthey, J. G. Checkelsky, N. P. Ong, et al., Nature **460**, 1101 (2009), URL <http://dx.doi.org/10.1038/nature08234>.
 - [9] Y. L. Chen, J. G. Analytis, J.-H. Chu, Z. K. Liu, S.-K. Mo, X. L. Qi, H. J. Zhang, D. H. Lu, X. Dai, Z. Fang, et al., Science **325**, 178 (2009), URL <http://www.sciencemag.org/content/325/5937/178.abstract>.
 - [10] Z. Alpichshev, J. G. Analytis, J.-H. Chu, I. R. Fisher, Y. L. Chen, Z. X. Shen, A. Fang, and A. Kapitulnik, Phys. Rev. Lett. **104**, 016401 (2010).
 - [11] P. Roushan, J. Seo, C. V. Parker, Y. S. Hor, D. Hsieh, D. Qian, A. Richardella, M. Z. Hasan, R. J. Cava, and A. Yazdani, Nature **460**, 1106 (2009), URL <http://dx.doi.org/10.1038/nature08308>.
 - [12] L. Fu and C. L. Kane, Phys. Rev. B **76**, 045302 (2007).
 - [13] X. Dai, T. L. Hughes, X.-L. Qi, Z. Fang, and S.-C. Zhang, Phys. Rev. B **77**, 125319 (2008).
 - [14] J.-W. Luo and A. Zunger, Phys. Rev. Lett. **105**, 176805 (2010).
 - [15] C. Brüne, C. X. Liu, E. G. Novik, E. M. Hankiewicz, H. Buhmann, Y. L. Chen, X. L. Qi, Z. X. Shen, S. C. Zhang, and L. W. Molenkamp, Phys. Rev. Lett. **106**, 126803 (2011).
 - [16] B. A. Bernevig, T. L. Hughes, and S.-C. Zhang, Science **314**, 1757 (2006), URL <http://www.sciencemag.org/content/314/5806/1757.abstract>.
 - [17] M. König, S. Wiedmann, C. Brüne, A. Roth, H. Buhmann, L. W. Molenkamp, X.-L. Qi, and S.-C. Zhang, Science **318**, 766 (2007), URL <http://www.sciencemag.org/content/318/5851/766.abstract>.
 - [18] X.-L. Qi, T. L. Hughes, and S.-C. Zhang, Phys. Rev. B **78**, 195424 (2008).
 - [19] A. M. Shuvaev, G. V. Astakhov, A. Pimenov, C. Brüne, H. Buhmann, and L. W. Molenkamp, Phys. Rev. Lett. **106**, 107404 (2011).
 - [20] C.-X. Liu, X.-L. Qi, H. Zhang, X. Dai, Z. Fang, and S.-C. Zhang, Phys. Rev. B **82**, 045122 (2010).
 - [21] F. Wilczek, Phys. Rev. Lett. **58**, 1799 (1987).

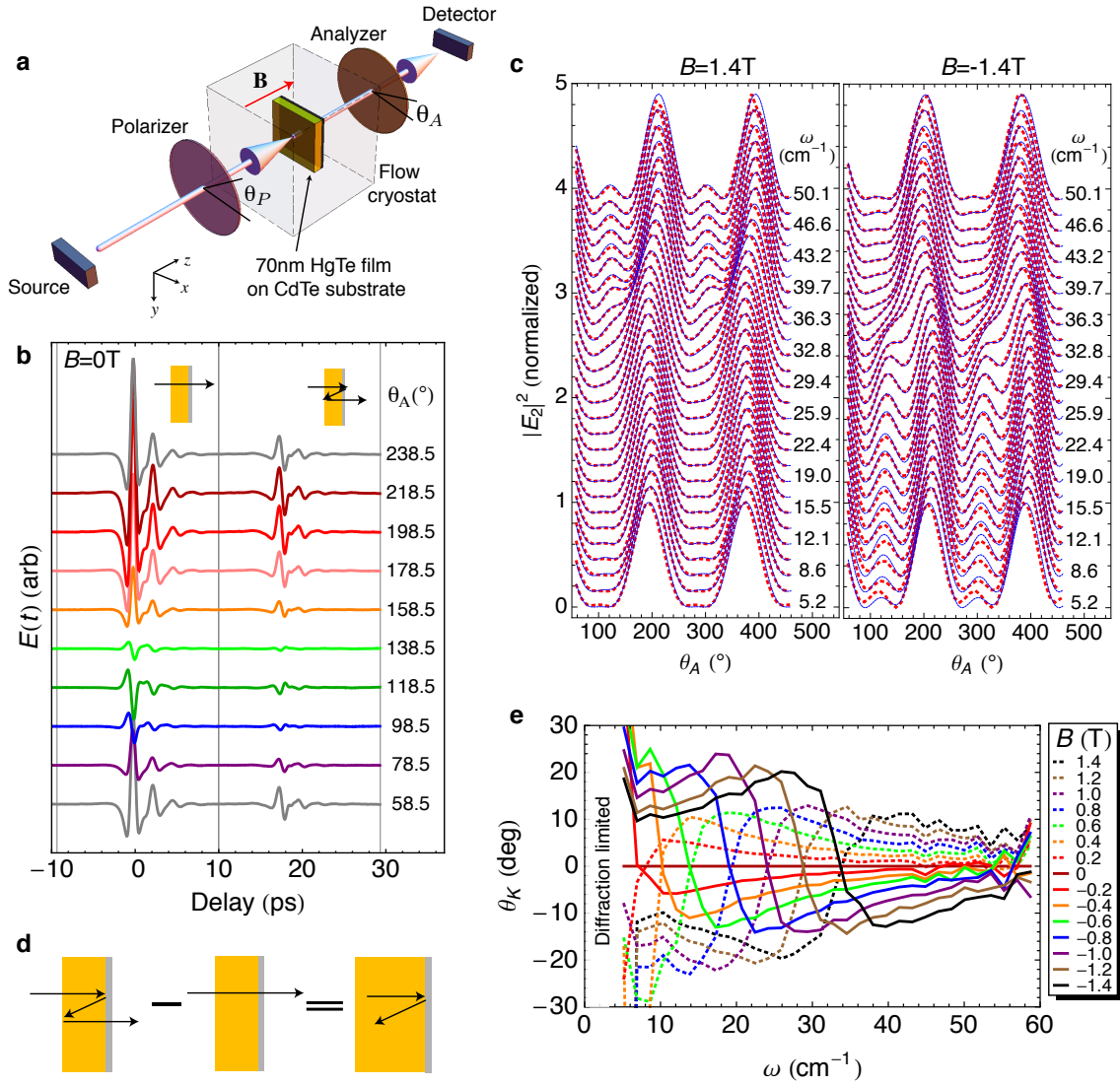


FIG. 1: **Time-domain measurement of the normal-incidence Kerr angle** (a) Illustration of the magneto-optical THz apparatus. θ_P was set to 51.2° throughout. (b) Subset of the angle-dependent measurements of the 1st and 2nd pulses. Vertical lines show the cuts used to separate the pulses into E_1 and E_2 . (c) Quality of fit used to determine the theoretical Faraday angle $\theta_{F,2}(\omega)$ for +1.4T and -1.4T. (d) Pictorial rationale for the expression $\theta_{F,2} - \theta_{F,1} = \theta_K$. (e) The measured Kerr angle for several magnetic fields.

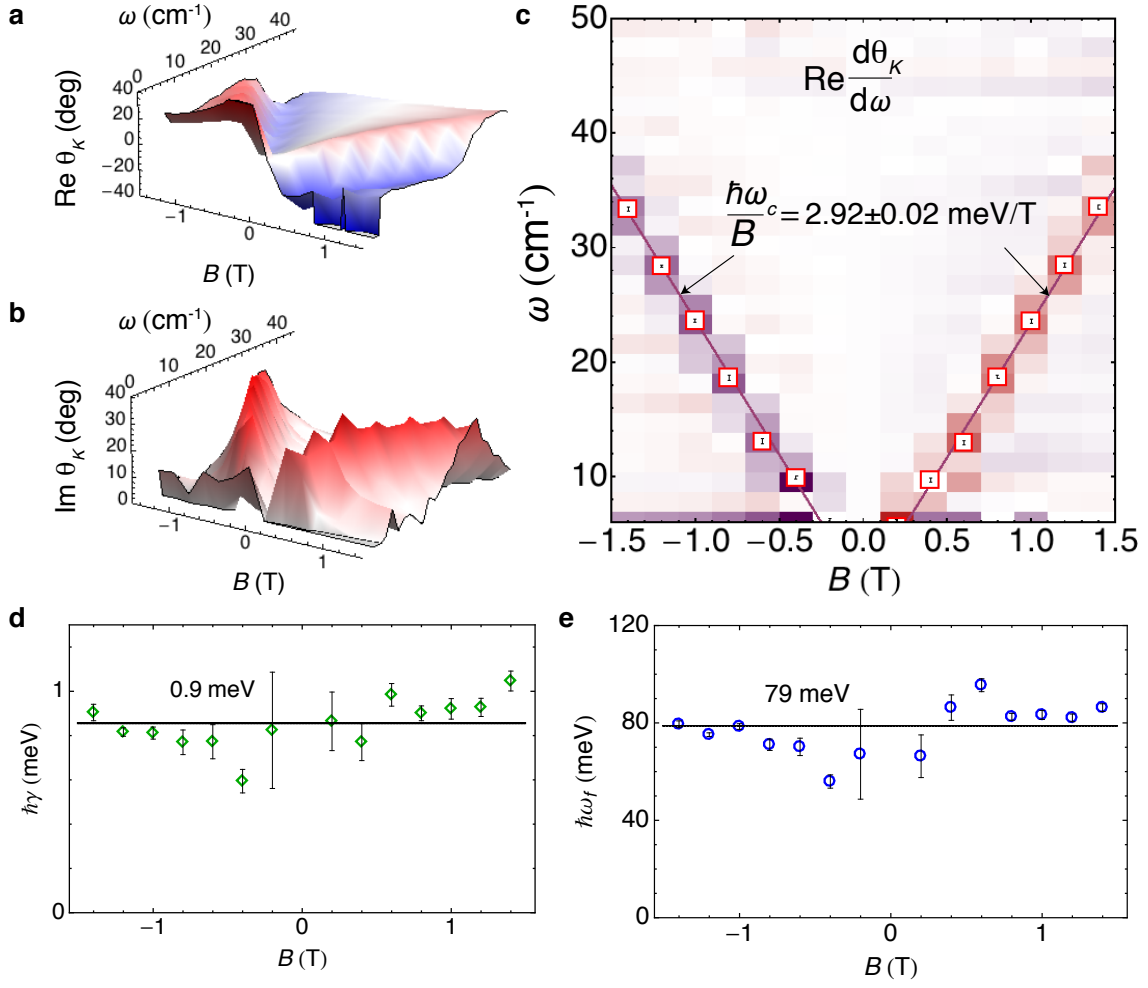


FIG. 2: **Properties of the surface-state cyclotron resonance** Real (a) and imaginary (b) Kerr angle $\theta_K(\omega, B)$ determined from terahertz ellipsometry. (c) The experimentally determined ω_c overlaying the experimental frequency derivative $\text{Re}d\theta_K/d\omega$, and a linear fit showing the B -linear CR behavior. (d,e) Fit parameters γ and ω_f .

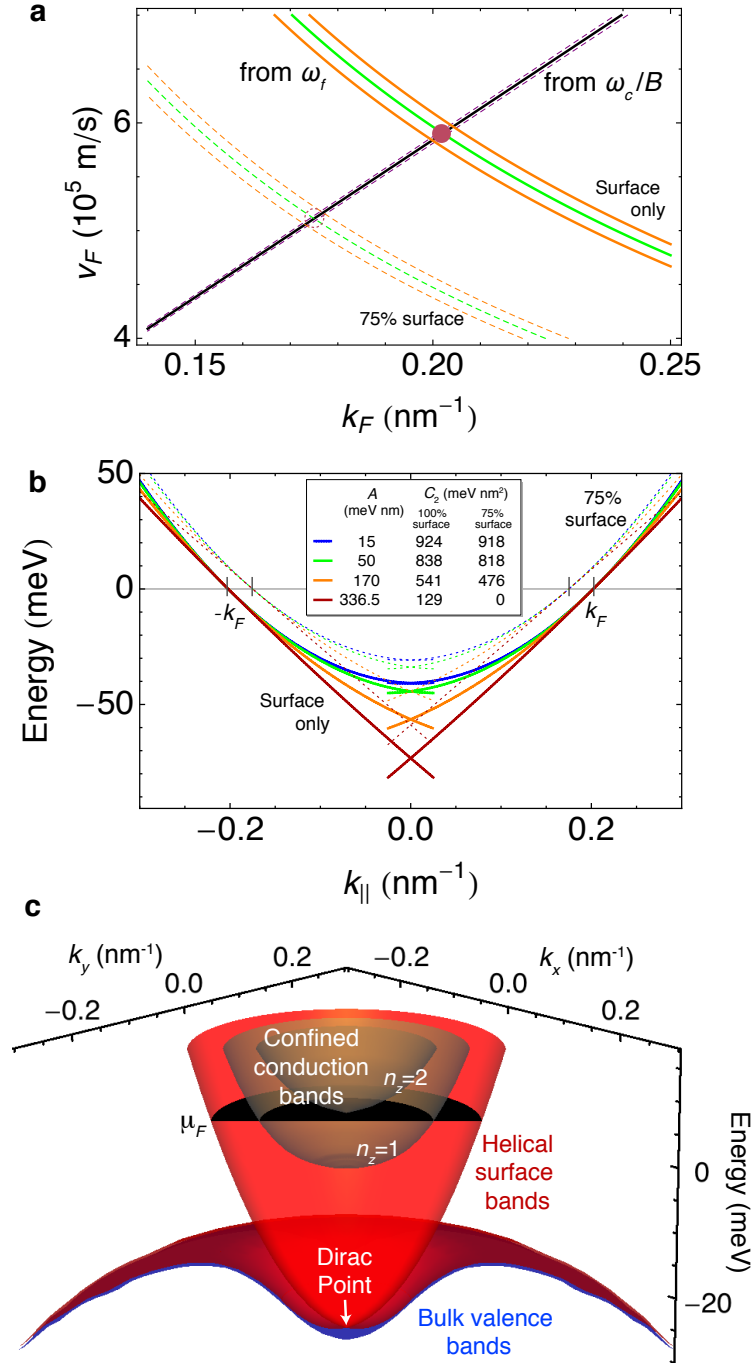


FIG. 3: **Dispersion of the surface state band** (a) Fermi parameters k_F and v_F consistent with the magneto-optical data assuming the CR is due solely to two identical surface states at the surface and interface. Dashed lines show the effect of breaking this assumption and allowing 25% of the Drude weight to be attributed to the confined conduction band states. (b) Possible realizations of the surface state model in [20] which are consistent with our observations for different choices of A and C_2 . (c) Dispersion of the surface state quasiparticles determined in this work with 75% surface state signal, $A = 25$ meV·nm, and $C_2 = 890$ meV·nm².